AD-A068 000 CORNELL UNIV ITHACA N Y DEPT OF MATERIALS SCIENCE A--ETC F/G 11/6
STRESS RELAXATION IN COILED RIBBONS OF FE40NI40P14B6 AND FE29NI--ETC(U)
JAN 78 D G AST, D J KRENITSKY

UNCLASSIFIED TR-3 NL

| OF |
AD
A068000

END
DATE
FILMED
6-79
DDC

(12) LEVEL II

STRESS RELAXATION IN COILED RIBBONS OF

$Fe_{40}Ni_{40}P_{14}B_6$ and $Fe_{29}Ni_{49}P_{14}B_6Si_2$

D.G. Ast & D.J. Krenitsky

Contract Number: NR039-151/N0014-77-C-0546

Technical Report #3

January 1978

SECURITY CLASSIFICATION OF THIS PAGE (When Data Entered)

REPORT DOCUMENTATION PAGE

READ INSTRUCTIONS BEFORE COMPLETING FORM

1. REPORT NUMBER: Technical Report No. 3
2. GOVT ACCESSION NO.:
3. RECIPIENT'S CATALOG NUMBER:

4. TITLE (and Subtitle): Stress Relaxation in Coiled Ribbons of $Fe_{40}Ni_{40}P_{14}B_6$ and $Fe_{29}Ni_{49}P_{14}B_6Si_2$.

5. TYPE OF REPORT & PERIOD COVERED: Technical Progress Report

6. PERFORMING ORG. REPORT NUMBER:

7. AUTHOR(s): D.G. Ast and D.J. Krenitsky

8. CONTRACT OR GRANT NUMBER(s):

9. PERFORMING ORGANIZATION NAME AND ADDRESS:
Mat. Sci. & Eng.; Bard Hall
Cornell Univ.; Ithaca, NY 14853

10. PROGRAM ELEMENT, PROJECT, TASK AREA & WORK UNIT NUMBERS:

11. CONTROLLING OFFICE NAME AND ADDRESS:

12. REPORT DATE: Jan. 78

13. NUMBER OF PAGES: 27

14. MONITORING AGENCY NAME & ADDRESS (if different from Controlling Office):

15. SECURITY CLASS. (of this report): Unclassified

15a. DECLASSIFICATION/DOWNGRADING SCHEDULE:

16. DISTRIBUTION STATEMENT (of this Report):
Distribution of this Document is Unlimited

17. DISTRIBUTION STATEMENT (of the abstract entered in Block 20, if different from Report):

18. SUPPLEMENTARY NOTES:

19. KEY WORDS (Continue on reverse side if necessary and identify by block number):
Metallic glass, Stress Relaxation

20. ABSTRACT (Continue on reverse side if necessary and identify by block number):
The stress relaxation in wound ribbons of metallic glasses is analyzed, using the elastic-plastic model. It is shown that an initial phase of load redistribution is followed by a quasi-steady state part. In all stages, stress relaxation follows an Eyring type flow law with $\Delta H \approx 2.5$ eV and $v^* = 400$ Å^3.

DD FORM 1 JAN 73 1473 EDITION OF 1 NOV 65 IS OBSOLETE
S/N 0102-LF-014-6601

Unclassified
SECURITY CLASSIFICATION OF THIS PAGE (When Data Entered)

STRESS RELAXATION IN COILED RIBBONS of $Fe_{40}Ni_{40}P_{14}B_6$ and $Fe_{29}Ni_{49}P_{14}B_6Si_2$

D. G. Ast and D. J. Krenitsky

Department of Materials Science and Engineering
Cornell University
Ithaca, New York 14853

ABSTRACT

The stress relaxation at elevated temperatures in coiled ribbons of Fe-Ni base metallic glasses is calculated for both power law creep and Eyring activated flow. The results are compared with experimental data on the spring back of coiled ribbons after various anneals. Good agreement is obtained for Eyring activated flow, but not for power law creep. Comparison with stress relaxation experiments on straight sections indicates that stress relaxation in coiled ribbons is largely due to transient creep.

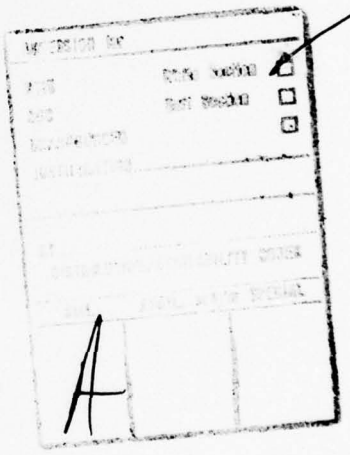

1.) Introduction

The tensile compliance of metallic glasses consists typically of three contributions: a) an instantaneous elastic part, b) a transient or anelastic part and c) a steady state or plastic part.[1] The transient part is largely, but not completely recoverable. The non-recoverable fraction of the transient compliance is on the order of 5% or less,[2] and and is ascribed to the relaxation of the quenched glass towards a more stable structure.[2] This contribution therefore decreases with the number of test cycles on a given specimen.[2]

The relative magnitude of the three contributions to the tensile compliance varies with temperature. At high temperatures ($T_g > T > T_g$ -20°C) the anelastic contribution becomes very large, about 200 times larger than the elastic contribution. In this narrow temperature range, metallic glasses behave therefore almost like glassy polymers. Sufficiently below T_g, the anelastic contribution is of the order of the instantaneous elastic contributions, or fractions thereof.

According to reference 2 the nature of the anelastic element at low temperatures (T_g-110° < T < T_g-210°C) and low stresses is Maxwellian, but at stresses higher than about a quarter of the yield stress a more complex behavior is observed.[2] Recently a more detailed analysis has shown that in Pd-Si glasses the recoverable (i.e. majority) and nonrecoverable (minority) part of the transient component can be modeled with a Maxwell element in series with a Voight element.[3]

The steady state or plastic deformation is viscous only at high temperatures (T_g-30 < T < T_g) where it follows the Vogel-Fulcher equation. Below this range, the temperature dependence of the plastic flow is usually expressed by an Arrhenius expression with a temperature dependent activation energy. The activation energy decreases rapidly below T_g-30°C and reaches an approximately constant value in the region where the viscosity is greater than about $10^{15}Nm^{-2}sec$. In the region T_g-210 < T < T_g-110°C the measured activation energy for Pd-Si based metallic glasses is 0.5 eV,[2] and 0.1 to 1 eV in Ni-P or Co-P based metallic glasses.[4]

The stress dependence of the plastic deformation is small and can, within the experi-

mental error, be satisfactorily described by both an Eyring model and by a power law.[2] The Eyring model yields an activation volume v* on the order of an atomic volume Ω.[1,2] Alternatively, the power law description, $\dot{\epsilon} = A\sigma^n$, fits the data with n=1.6 in Pd base glasses[2] and 1 in Ni-P.[3] For temperatures closer than about 10°C to T_g, the stress dependence increases rapidly and v* may reach 100 Ω.[1]

Most of the reported mechanical data on amorphous alloys pertain to Pd-Si based metallic glasses which can be prepared more easily than the Ni-Fe based variety. In view of this situation we studied the relaxation behavior of Ni-Fe base metallic glasses in considerable detail.[5] This paper reports an analysis of the transient deformation which, as we will show, dominates the stress relief in practical annealing situations such as is encountered in the annealing of wound transformer cores.

2.) Experimental

Two types of experimental data are available for an analysis of the stress relaxation behavior of amorphous $Fe_{40}Ni_{40}P_{14}B_6$ (Tradename Allied Metglas #2826). These are stress relaxation data from tensile tests[5] and spring back measurements on 2826 ribbons coiled into rings prior to anneal.[6,7]

A typical result of a stress relaxation test under tension is shown in Fig. 1, which illustrates the relation between stress (vertical axis) and strain rate (horizontal axis) for four different initial stress levels. It can be seen that the $\log_{10} \sigma$ vs $\log_{10} \dot{\epsilon}$ relation consists phenomenologically of three parts, the borders between which are indicated by arrows in Fig. 1. Part 1 commences immediately after termination of loading and is characterized by an extreme sensitivity of the strain rate to stress. At 270°C, this part is completed in about 60 sec. Part 2 is the transient or anelastic deformation, which eventually merges into part 3, the steady state or plastic deformation. The transition between part 2 and part 3 is gradual and at 270°C occurs around 5 h, give or take a factor of 2. Part 3, the steady state deformation, is very accurately described by a power law with a stress exponent of about 4. A detailed investigation reveals that the stress exponent of a well annealed sample (T_{anneal}=300°C)

tested repeatedly at 270°C changes slightly with the number of load cycles rising from about 3.7 after the first loading to about 4.3 after the 6th loading. These changes are too small to be detected in Fig. 1 and are therefore shown separately in Fig. 2.

As the temperature is lowered, the time to reach steady state deformation increases very rapidly so that for practical time intervals this section of the log σ vs log $\dot{\epsilon}$ curve soon becomes unobservable.

Tests on ribbons coiled into rings prior to anneal are easily carried out and a number of investigators have used these tests as a qualitative means to check stress relief in wound ribbons. The most detailed measurements, by far, are those by Graham, Egami, Williams and Takei,[6] whose measurements are reproduced in Figs. 3, 4 and 5. Their specimens were coiled into rings of 6.5 mm radius prior to anneal at various temperatures and times. After each anneal, the equilibrium radius of curvature was measured. Stress relaxation was then plotted on a scale from 1, corresponding to the initial stress, to 0, corresponding to complete stress relaxation or zero spring back. These investigators reported that they tried unsuccessfully to deduce activation energies from the data, or to fit the curves to conventional kinetic equations.

In the following section we will analyze their data and show that they can be accounted for by an Eyring type flow.

3.) Analysis

The task at hand is to evaluate the time dependent stress distribution in the ribbon, as progressive relaxation changes the initial linear elastic stress distribution introduced by coiling at the time t=0. Out of the many models proposed for relaxation, two flow laws were investigated in detail in this analysis. The respective laws were an Eyring activated state model:

$$\dot{\epsilon} = \dot{\epsilon}_o \exp(-\Delta H/kT)2\sinh(v^*\sigma/kT) \tag{1}$$

and a power law of the form:

$$\dot{\epsilon} = \dot{\epsilon}_o \exp(-\Delta H/kT)(\sigma/\sigma_o)^n \tag{2}$$

If the stress distribution $\sigma(z,t)$ is known, the stress distribution at the time $t+\Delta t$, is given by

$$\sigma(z,t+\Delta t) = \sigma(z,t) - E \cdot \dot{\varepsilon}(z,t) \cdot \Delta t \tag{3}$$

where E is the elastic modulus (Youngs modulus). For $\Delta t \rightarrow 0$, one obtains, with flow laws (1) and (2):

$$\frac{\partial \sigma}{\partial t} = -2E\dot{\varepsilon}_o \exp\ (\Delta H/kT)\sinh(v^*\sigma/kT) \tag{4}$$

and

$$\frac{\partial \sigma}{\partial t} = -E\dot{\varepsilon}_o(\sigma/\sigma_o)^n \exp(-\Delta H/kT) \tag{5}$$

The boundary condition is that for t=0 the stress distribution is linear, i.e.

$$\sigma(z,0) = (2z/d)\sigma_o$$

where z is the coordinate perpendicular to the plane of the ribbon starting at the neutral axis, d the thickness of the ribbon and σ_o the elastic surface stress at t=0. The general solution of equation (4) is given by:

$$\frac{\sigma}{\sigma_o} = \frac{kT}{v^*\sigma_o} \ln \frac{1+f(z)f(t)}{1-f(z)f(t)} \tag{6}$$

where

$f(t)=\exp(-2E\dot{\varepsilon}_o \exp(-\Delta H/kT)v^*/kT)$

and

$$f(z) = \frac{\exp(\sigma(z,0)v^*/kT)-1}{\exp(\sigma(z,0)v^*/kT+1}.$$

With the help of hyperbolic functions Eq. (6) can be written more concisely as:

$$(\sigma/\sigma_o) = (kT/v^*\sigma_o)\ 2\ \mathrm{arth}[\ \mathrm{th}(\sigma(z,0)/2kT)\ \exp(-2E\dot{\varepsilon}_o\exp(-\Delta H/kT)v^*/kT)\ ] \tag{7}$$

The solution for power law creep is simpler and given by:

$$(\sigma/\sigma_o) = \left[\ 1 - \frac{E\dot{\varepsilon}_o\exp(-\Delta H/kT)(n-1)t}{\sigma_o^n\ \sigma(z,0)^{1-n}}\ \right]^{1/1-n} \tag{8}$$

These equations have been evaluated with the aid of a PDP 12 computer and Figs. 6 and 7 show calculated stress distributions in coiled ribbons at various times for the two flow laws. The values chosen for the flow parameters, $v^* = 400\ (\text{Å})^3$ and n = 13 are typical for what one obtains from an analysis of experimental data. The general behavior in Figs. 6 and 7 is quite similar except at low stresses where the power law gives a much slower stress relief with

time. This behavior generates, as we will see, a "tail" in the time dependent moment which is characteristic for power law creep.

The stress distributions (7) and (8) can be used to calculate the time dependent moments which are directly related to the observed radii of curvature:

$$M(t)/M(t_o) = \int_o^{d/2} \sigma\,(z,t)zdz \Big/ \int_o^{d/2} \sigma\,(z,0)zdz \qquad (9)$$

This integration was carried out numerically on a PDP 12 computer, except for the case n=4 which can be integrated easily in closed form, yielding:

$$M(t)/M(t_o) = (3/2\phi)[(1+\phi)^{2/3}-1] \qquad (10)$$

$$\text{with: } \phi = [3E\dot{\varepsilon}_o \exp(-\Delta H/kT)] \cdot [t/\sigma_o]$$

σ_o is given by the geometry. The other parameters i.e. $\dot{\varepsilon}_o$, ΔH, and v^* or, alternatively n, which enter Eq. (9) were varied in an attempt to match the experimental data. In the initial stage of parameter fitting, we found it convenient to approximate the actual stress distribution with two linear sections (see Fig. 8). The moment is then simply given by:

$$M(t)/M_o = (1.5 \cdot \sigma(d/2,t) - (0.5 \cdot \sigma(d,t)^3) \qquad (11)$$

where $\sigma(d/2,t)$ is given by Eq. (7) and (8) respectively. The approximation is fairly accurate even for moderate stress dependence (n=4, see Figs. 9 and 10) and becomes quite accurate at higher stress dependences (n=13) where the deviations between the actual and the approximate stress dependence become small.

4.) Results

Comparisons between the results of the calculations and the experimental data are shown in Figs. 9-14.

It was found that the stress relief in coiled ribbons could not be described with a power type flow law. Figs. 9 and 10 show the best fit obtained for n=4; i.e. the flow law which describes the steady state or plastic deformation part of the stress relaxation curve of Fig. 1. The calculated curves fall faster with the time than experimentally observed, indicating

that stress relaxation in coiled ribbons is not caused by plastic flow. Treating n as an adjustable parameter did not improve the fit. A typical result is shown in Fig. 11. The choice of n=13 generates a good fit for the 150°C annealing data, but fails to represent the slope of the experimental data at other annealing temperatures. In addition one finds that the shift of the annealing curves with temperature can not be described with a single activation energy.

The results obtained with an Eyring type hyperbolic flow law are depicted in Figs. 12-14, which show both the results obtained with 2826 (composition $Fe_{40}Ni_{40}P_{14}B_6$) and with 2826 B (composition $Fe_{29}Ni_{49}P_{14}B_6Si_2$).

Figure 12 shows that the long term ($0.1 < t < 1000$ h) annealing of coiled 2826B ribbons can be matched successfully with such a flow law. The parameters entering the calculation were $\dot{\epsilon}_o = 9.10^{18}h^{-1}$; ΔH=2.46 eV (56.6Kcal/mol); and $v^* = 400$ (Å).^{3} The accuracy with which these parameters can be determined is about 10% in the case of $\dot{\epsilon}_o$and 5% or better in the case of ΔH and v^*. Besides a good overall matching, the calculated curves reproduce previously unnoticed trends in the experimental data such as a slight negative curvature of the annealing curves at lower annealing temperatures. The slight deviation in the position (but not the slope) of the 250° isotherm is probably a real effect and will be discussed later.

The predictions for the short term annealing behavior of 2826B, using the same set of parameters, is shown in Fig. 13. The good agreement between theory and experiment indicates that the same process that controls the long term annealing behavior also controls the short term annealing behavior down to ~ 7 min., i.e. the shortest annealing times studied.

Next, we present the results obtained on 2826. Figure 14 shows that very good fits can be obtained for T=150 and 200°C, but that for T=225 and T=250°C deviations set in at longer annealing times. There are not enough experimental data to fix the onset of these deviations reliably for T=225°C. At 250°C, the deviations set in somewhere between 5.6 h (the last data point fitted by the theoretical prediction) and 45 h (the first data point to show an unambiguous deviation). The direction of the deviations are towards larger times; i.e.

annealing proceeds slower than predicted. The values entered for 2826 were $\dot{\epsilon}_o = 6.10^{19}$; $\Delta H = 2.414$ eV (55.6kcal); and $v^* = 360$ (Å).[3]

5.) Discussion

The deviations observed in 2826 annealed for long times at high temperatures are easily understood with the aid of Fig. 1 which shows that after several hours time, transient creep is replaced by steady state creep (the exact time at which this transition occurs is stress dependent and for this reason the two sets of data can not be compared directly). Extrapolation of the transient creep equation to low stress levels results in an overestimate of the creep rate which accounts for the observed deviations. It would be desirable to have more accurate stress relaxation data on coiled ribbons at high temperatures and long annealing times to confirm this interpretation by a direct analysis of the experimental data along the lines of Eq. (7).

The results on both plastic or steady state and the transient or anelastic creep in Fe-Ni based metallic glasses are somewhat surprising. In the plastic range, the very high precision of the stress relaxation data allows an experimental discrimination between a power law description and a hyperbolic flow model. Such an analysis shows that a power law with $n \sim 4$ fits the experimental data within the small experimental errors whereas a hyperbolic fit results in small but systematic deviations just outside the experimental scatter. (If one nevertheless analyzes such a fit one finds v^* for steady state creep on the order of an atomic volume which agrees with the observation on Pd-Si based glasses). The stress exponent of ~ 4, is unusual in view of the results on both Pd-Si based glasses ($n=1.6$) and Ni-P ($n=1$). It also does not agree with the prediction of the free volume theory which predicts $n=1$.[8] Dislocation models, of course, can easily account for the observed steady state creep exponent.

In the transient or anelastic deformation, considerable rearrangement must be involved on on atomic scale, as indicated by the large activation volume ($\sim$ 20 atomic volumes). The good matching of the calculated and experimental slopes at all temperatures indicate that v^* does not depend on temperature in the temperature range investigated.

The activation energy for transient creep of ~ 2.4 eV appears high compared to the reported activation energy for steady state creep in Fe-Ni base alloys (Q=0.35 eV in Ni-P), but matches, as is to be expected, those measured for internal friction (2.2-2.6 eV). The deviation between calculation and experiment observed at 250°C in 2826B (but not in 2826) could indicate a shift to higher activation energies as T approaches T_g. Such shifts are commonly observed in polymers if $T > T_g$-30°C. It is conceivable that the large structural instability of metallic glasses, relative to polymers, gives rise to such effects at temperatures which are in the order of T_g-100°C. To settle this question conclusively, data at higher annealing temperatures are needed. At the moment, the only activation energy available for the high temperature behavior of 2826 is the activation energy of crystallization (3.9 eV[9] at 400°C).

The activation energy for transient creep of 2826B is about .05 eV higher than that of 2826, a difference which is likely within experimental error. The trend, however, follows the observation on the activation energies for crystallization which increases with the number of atomic species in the alloy.[9]

By replotting the transient portion of Fig. 1 in a suitable coordinate system, one can show in an independent way that the anelastic relaxation follows roughly a hyperbolic flow law with a v* of about 400 (Å).[3]

The maximum, initial stress levels in the coiled ribbons investigated here are only about 1/3 of the initial stress levels in the tensile relaxation specimen of Fig. 1 so that a direct comparison of the relaxation behavior can not be carried out.

This is illustrated by the preexponential factor in the transient creep equation which depends on the initial loading in the specimen. The reasons for this can be seen from Fig. 1 which shows relaxation of 2826 in a tensile arrangement at four different load levels. The transients are quite similar, i.e. relaxation follows the same basic flow law. However, the stress relaxation at a lower load level does not fall on the extension of stress relaxation initiated at a higher stress level. Rather the translation at different load levels occurs along a

line which approximately parallels the steady state creep curve. The preexponential factor $\dot{\epsilon}_o$ therefore changes with stress in an approximately powerlike fashion, with a stress exponent of 4 if σ is normalized relative to σ_o.

6.) Summary

The stress relaxation process in coiled ribbons of Fe-Ni based metallic glasses has been analyzed.

It is found that the stress relaxation is almost entirely due to transient, nonsteady state, deformation which follows a hyperbolic flow law. The activation energies are 2.41 eV for 2826 and 2.46 eV for 2826B. The activation volumes are 360 $(\text{Å})^3$ in 2826 and 400 $(\text{Å})^3$ in 2826B.

Steady state creep is only reached after very long anneals at high temperatures and at stress levels of 10% or less of the initial stress level.

Acknowledgments

This research was supported by the Office of Naval Research under Contract NR039-151 and by the Material Science Center at Cornell.

References

1) H. S. Chen and M. Goldstein, J. Appl. Phys. 43 (1972) 1642.

2) R. Maddin and T. Masumoto, Mat. Sci. Eng. 9 (1972) 153.

3) T. Murat, H. Kimura and T. Masumoto, Scripta Met. 10 (1976) 705.

4) J. Logan and M. F. Ashby, Acta Met., 22 (1974) 1074.

5) T. D. Hadnagy, D. J. Krenitsky, D. G. Ast and C. Y. Li, Scripta Met. 12 (1978) 45.

6) C. D. Graham, Jr., T. Egami, R. S. Williams and Y. Takei, Magnetism and Magnetic Materials, AIP Conference Proc. #29 (1975), Eds. J. J Becker, G. H. Lander and J. J. Rhyne, p. 218.

7) L. A. Davis, R. Ray, C. P. Chou and R. C. O'Handley, Scripta Met. 10 (1976) 541.

8) F. Spaepen, Acta Met., 25 (1977) 407.

9) F. E. Luborsky, Mat. Sci. Eng., 28 (1977) 139.

Figure Captions

Fig. 1 Log_{10} of stress vs. log_{10} of strain rate as measured in a tensile test stress relaxation experiment. Results are shown for four different initial load levels. Test temperature is 270°C. The specimen was preannealed at 300°C to stabilize the structure.

Fig. 2 Stress exponent and preexponential factor as measured in repeated tensile test stress relaxation experiments on one specimen. Test temperature is 270°C.

Fig. 3 Short term annealing behavior of 2826B measured from the spring back of coiled ribbons. Data from Ref. 6.

Fig. 4 Long term annealing behavior of 2826B measured from the spring back of coiled ribbons. Data from Ref. 6.

Fig. 5 Long term annealing behavior of 2826 measured from the spring back of coiled ribbons. Data from Ref. 6.

Fig. 6 Calculated time dependent stress distribution in the ribbon, measured from the neutral axis. The calculation assumes that transient creep follows a hyperbolic flow law with $v^*=400$ $(Å)^3$.

Fig. 7. Calculated time dependent stress distribution in the ribbon measured from the neutral axis. The calculation assumes that transient creep follows a power law with $n=13$.

Fig. 8 Approximation used for the closed solution of Eq. 11 for $M(t)/M(0)$.

Fig. 9 Stress relief in coiled ribbons, assuming a power law with $n=4$ for transient creep. Solid lines are calculated, using the approximation indicated in Fig. 8. Dashed lines connect experimental results.

Fig. 10 Stress relief in coiled ribbons, assuming a power law with $n=4$ for transient creep. Solid lines are calculated numerically. Dashed lines connect experimental results.

Fig. 11 Stress relief in coiled ribbons, assuming a power law with n=13 for transient creep. Solid lines are calculated numerically. Dashed lines connect experimental results.

Fig. 12 Stress relief in coiled ribbons, assuming a hyperbolic flow law with $v^* = 400$ $(Å)^3$, $\Delta H=2.46$ eV, $\dot{\varepsilon}_o = 9.10^{18}$ for transient creep. Long term behavior. Solid lines are calculated numerically. Dashed lines connect experimental results.

Fig. 13 Stress relief in coiled ribbons, assuming a hyperbolic flow law with $v^* = 400$ (Å), $\Delta H=2.46$ eV, $\dot{\varepsilon}_o = 9.10^{18}$ for transient creep. Short term behavior. Solid lines are calculated numerically. Dashed lines connect experimental results.

Fig. 14 Stress relief in coiled ribbons, assuming a hyperbolic flow law with $v^* = 360$ $(Å)^3$, $\Delta H=2.41$ eV, $\dot{\varepsilon}_o = 6.10^{19}$ for transient creep. Long term behavior. Solid lines are calculated numerically. Dashed lines connect experimental results.

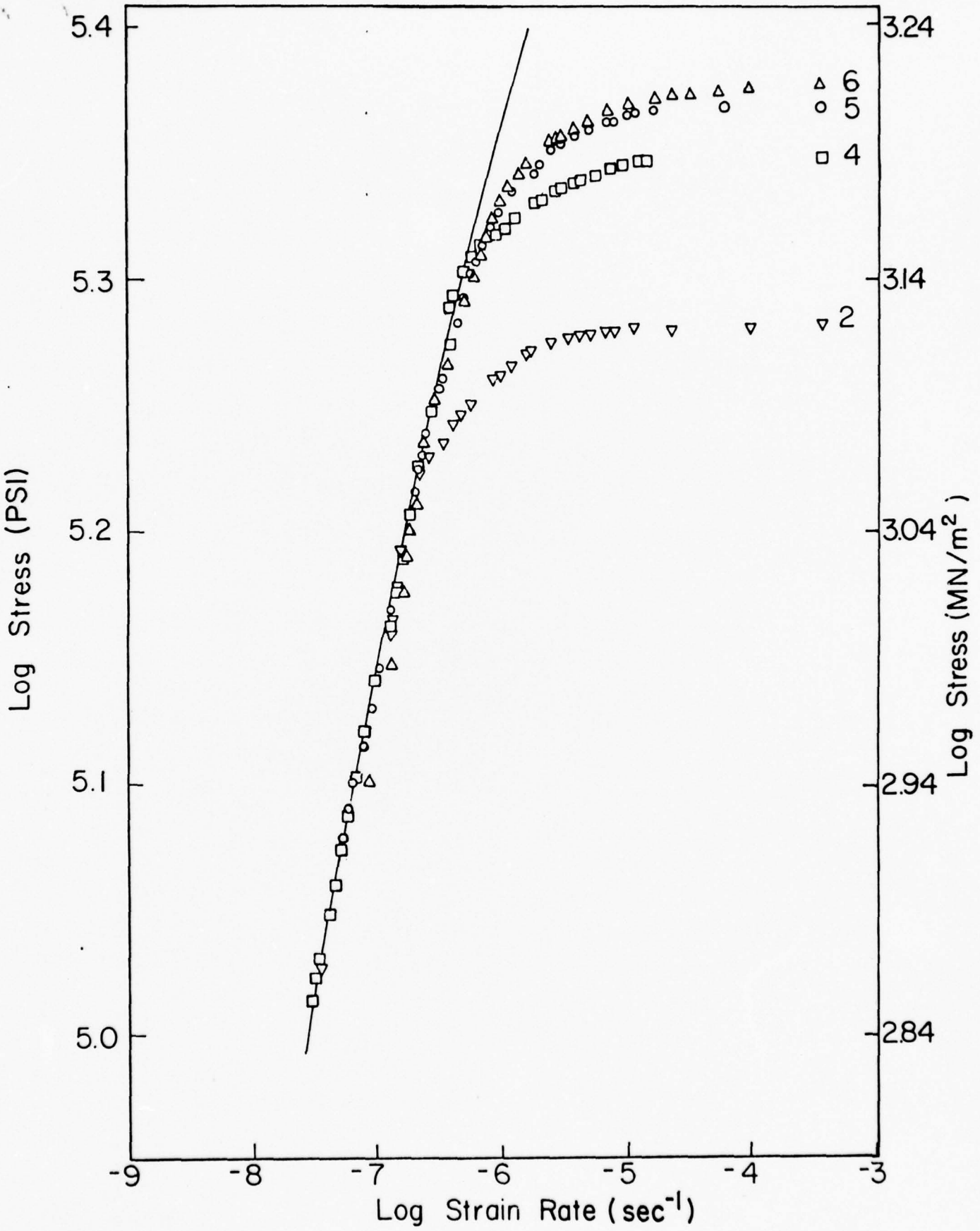
5.4
5.3
5.2
5.1
5.0
Log Stress (PSI)
3.24
3.14
3.04
2.94
2.84
Log Stress (MN/m^2)
6
5
4
2
-9
-8
-7
-6
-5
-4
-3
Log Strain Rate (sec^{-1})

FIGURE 1

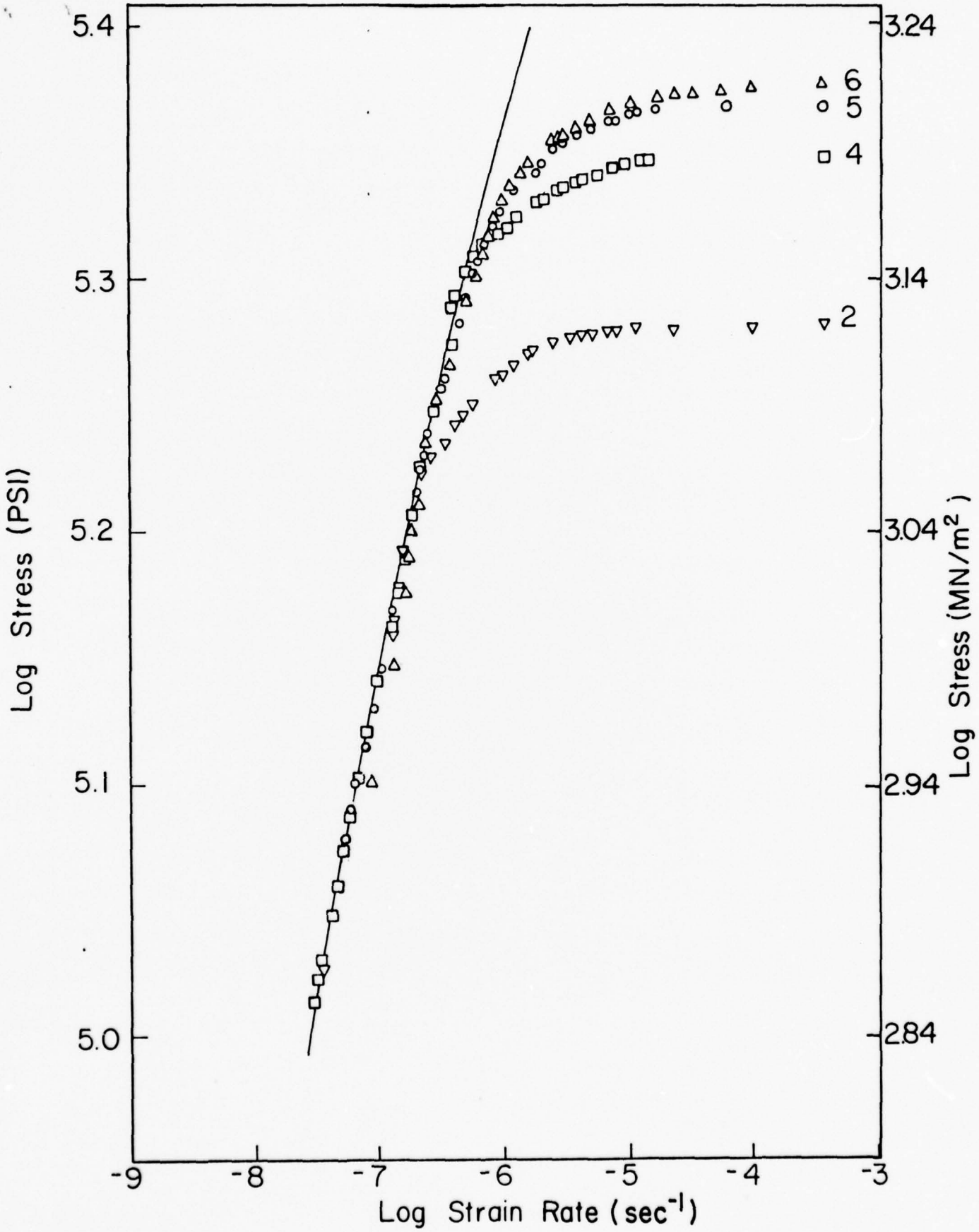
5.4
5.3
5.2
5.1
5.0
3.24
3.14
3.04
2.94
2.84
Log Stress (PSI)
Log Stress (MN/m^2)
6
5
4
2
-9
-8
-7
-6
-5
-4
-3
Log Strain Rate (sec^{-1})

FIGURE 1

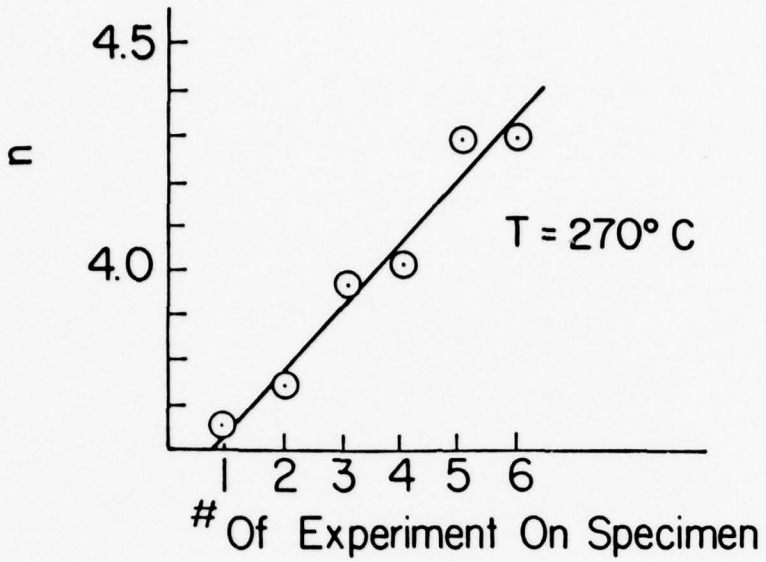
4.5
4.0
n
T = 270° C
1 2 3 4 5 6
Of Experiment On Specimen

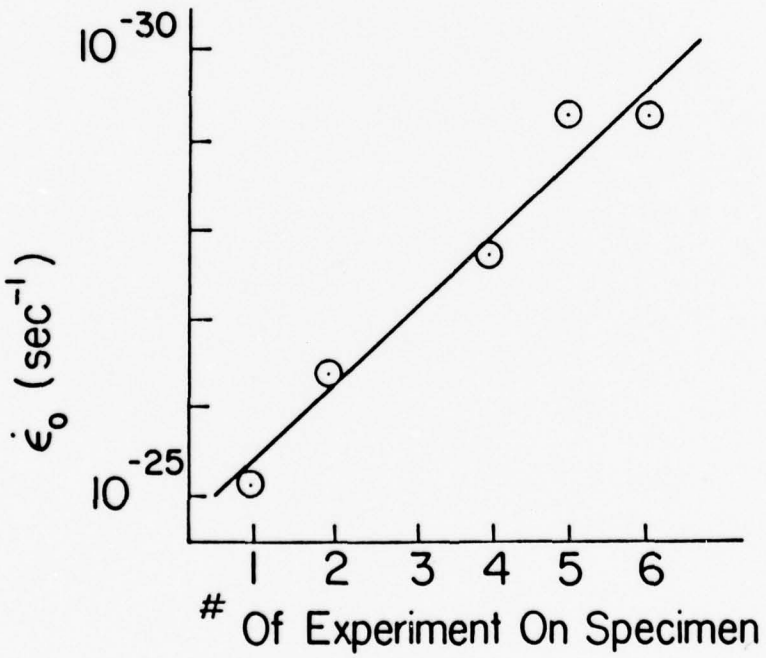
10^{-30}
10^{-25}
$\dot{\epsilon}_o$ (sec^{-1})
1 2 3 4 5 6
Of Experiment On Specimen

FIGURE 2

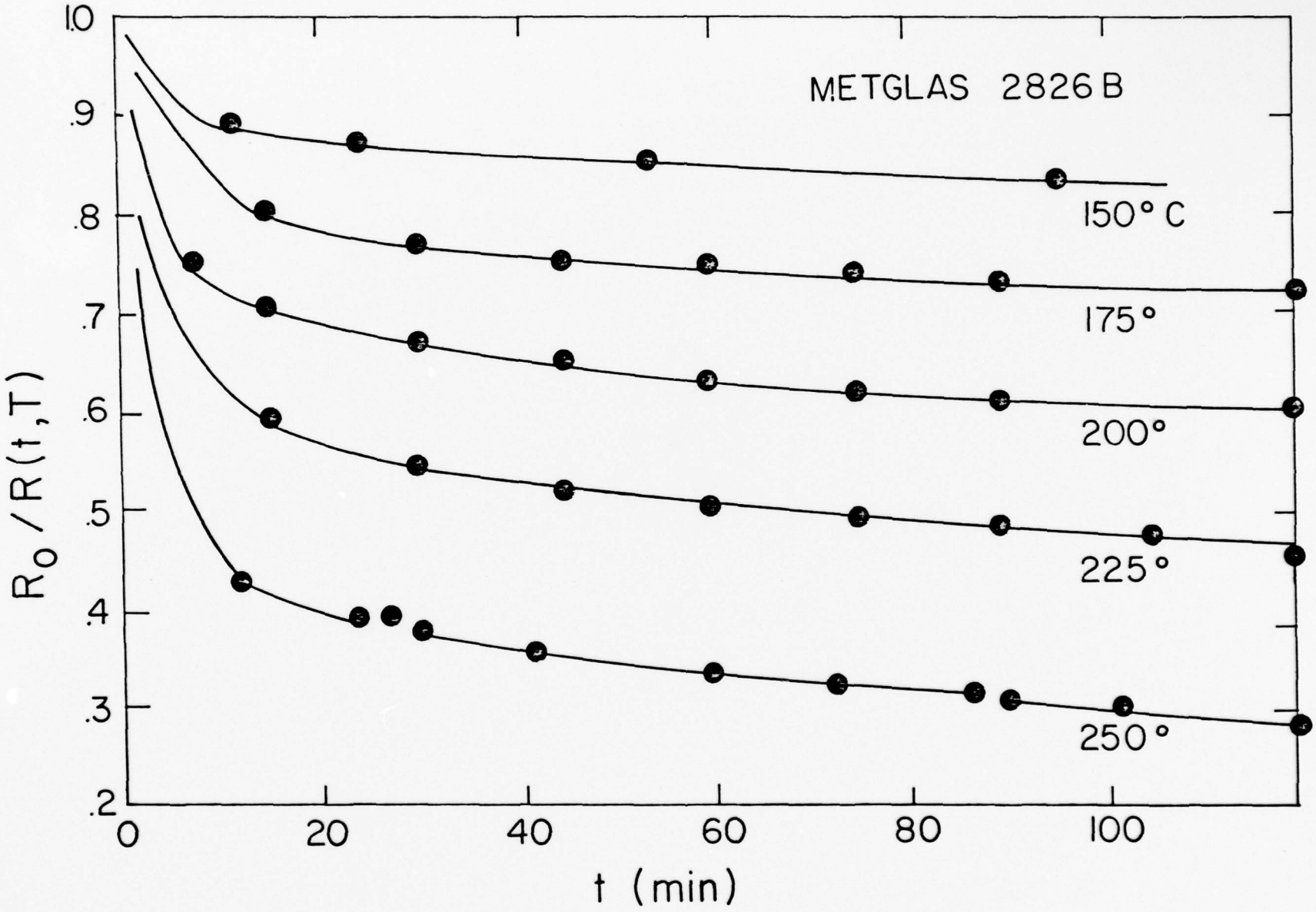
METGLAS 2826 B
150° C
175°
200°
225°
250°
$R_0 / R(t,T)$
t (min)
1.0
.9
.8
.7
.6
.5
.4
.3
.2
0
20
40
60
80
100

FIGURE 3

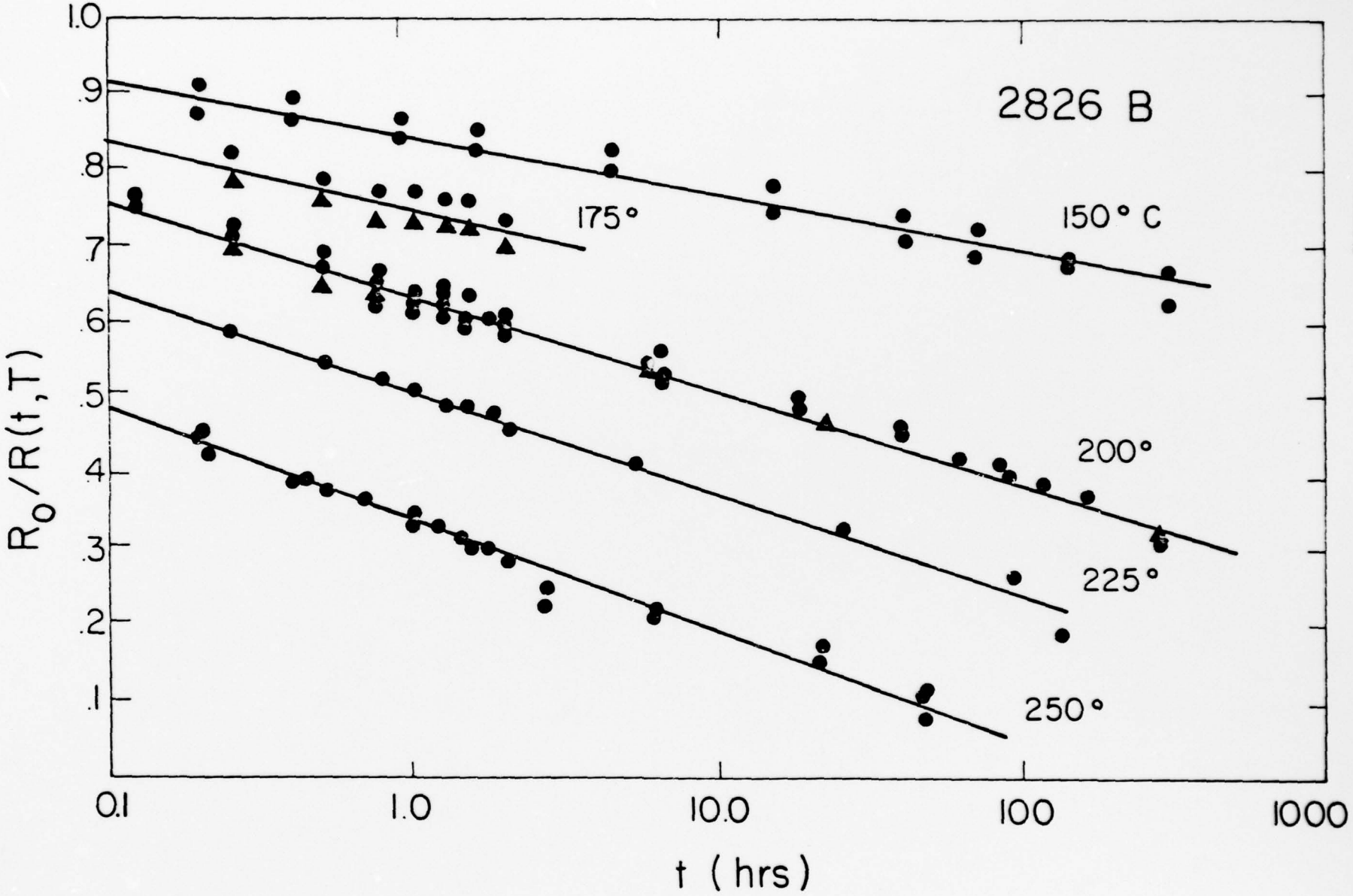
2826 B
150° C
175°
200°
225°
250°
$R_o/R(t,T)$
t (hrs)
1.0
.9
.8
.7
.6
.5
.4
.3
.2
.1
0.1
1.0
10.0
100
1000

FIGURE 4

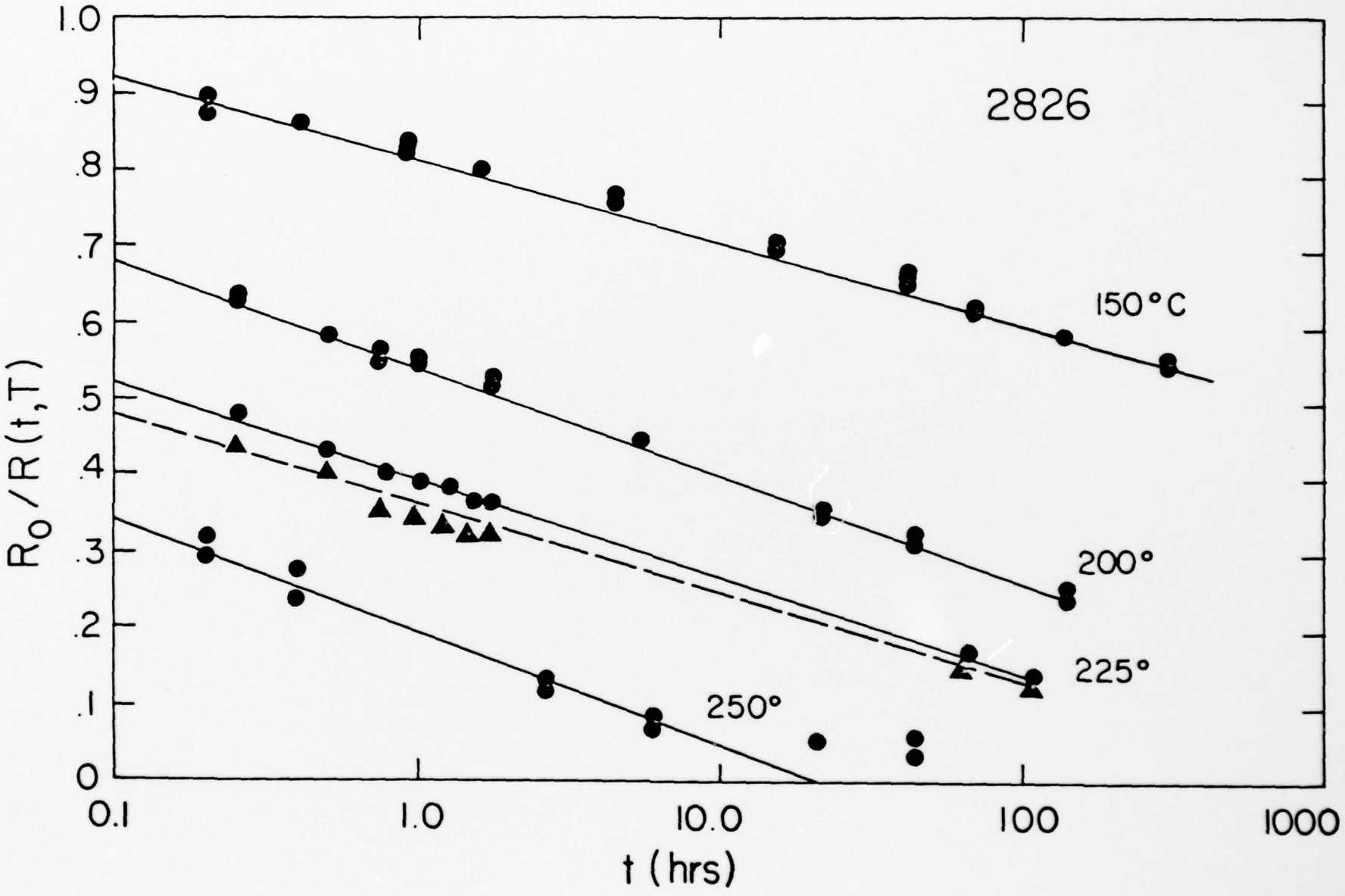
2826
150°C
200°
225°
250°
$R_o/R(t,T)$
t (hrs)
1.0
.9
.8
.7
.6
.5
.4
.3
.2
.1
0
0.1
1.0
10.0
100
1000

FIGURE 5

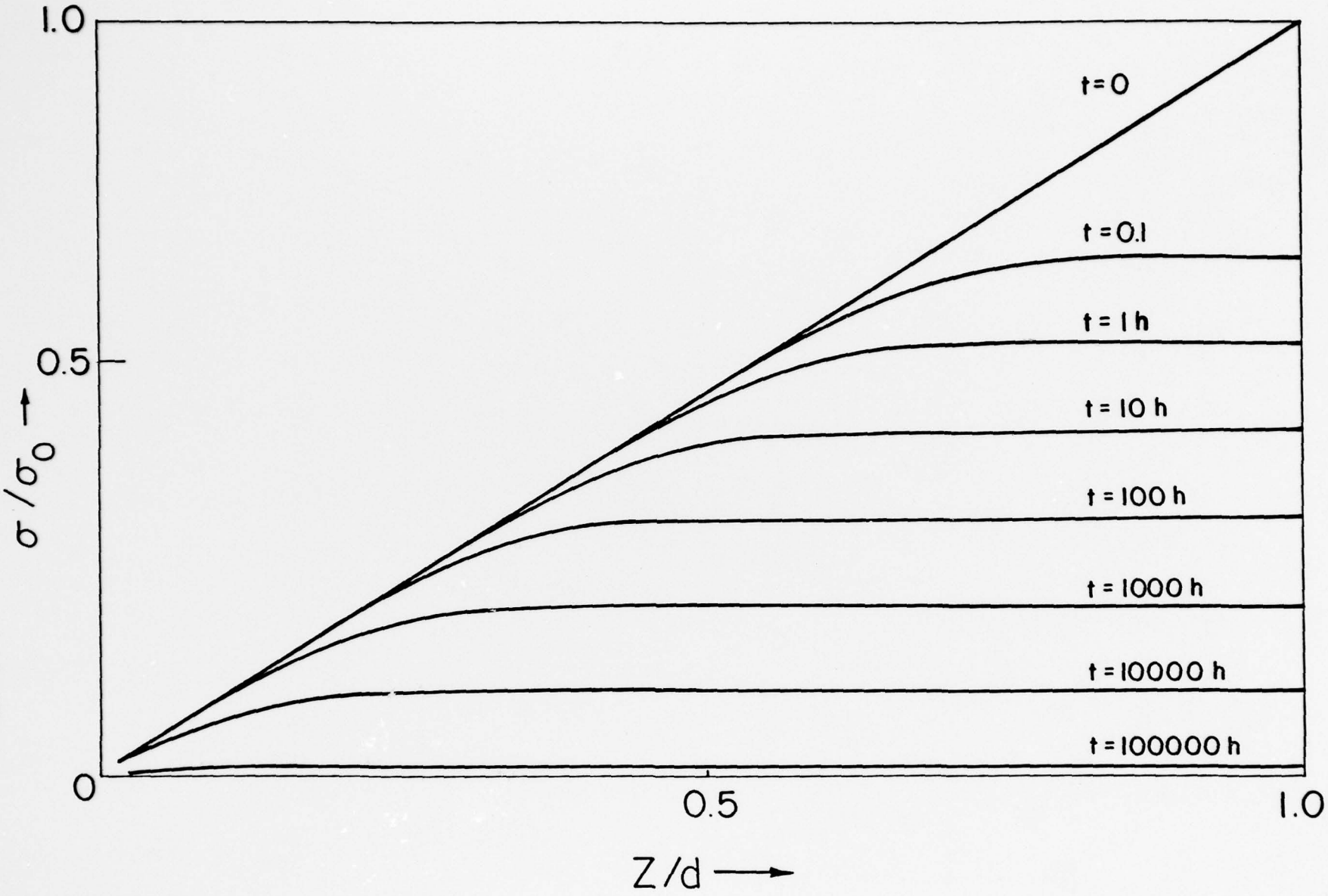
1.0
0.5
0
σ /σ0 →
0.5
1.0
Z/d →
t=0
t=0.1
t=1h
t=10 h
t=100 h
t=1000 h
t=10000 h
t=100000 h

FIGURE 6

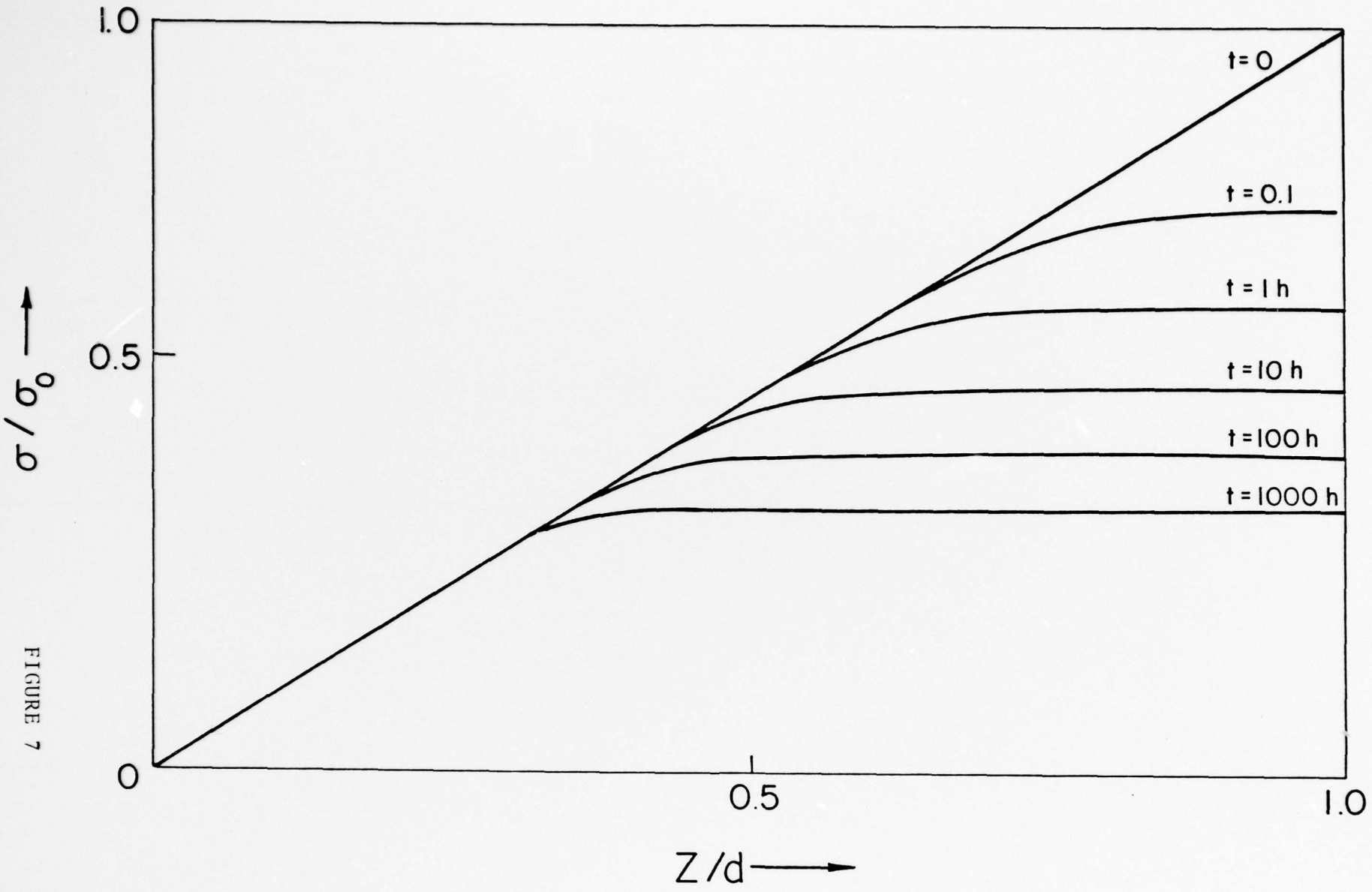

FIGURE 7

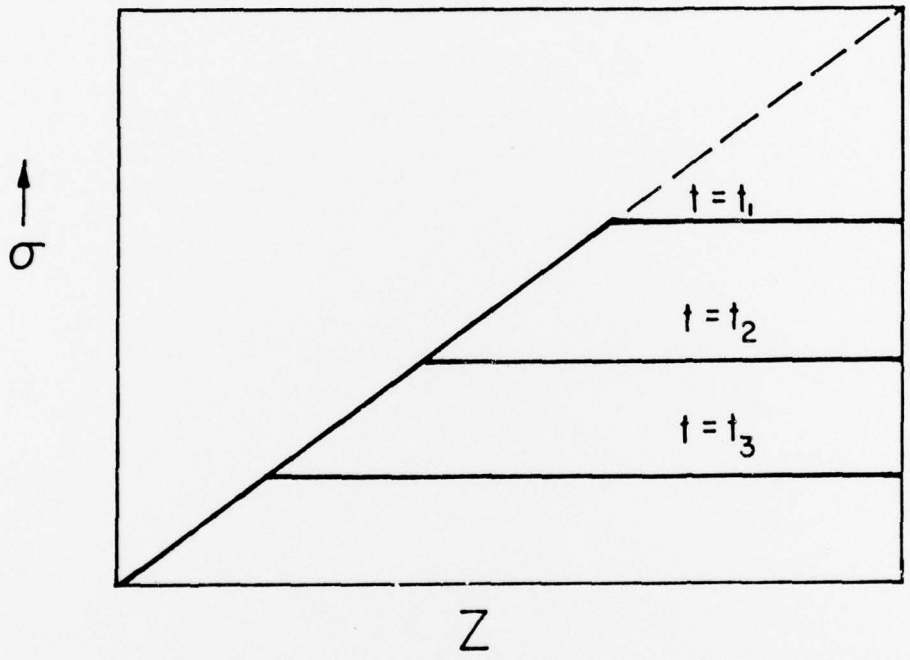

FIGURE 8

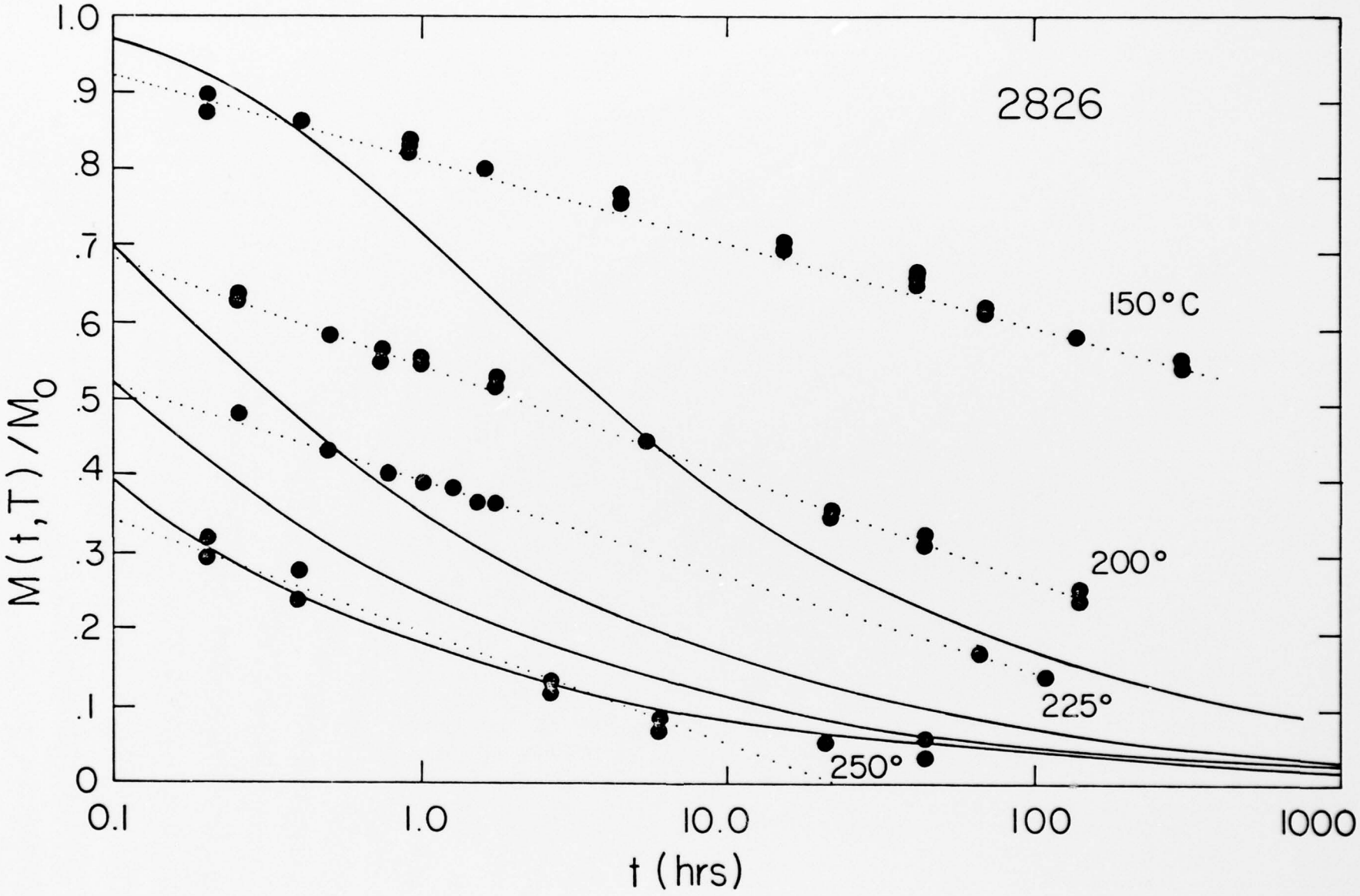
2826
150°C
200°
225°
250°
M(t,T)/M0
t (hrs)
1.0
.9
.8
.7
.6
.5
.4
.3
.2
.1
0
0.1
1.0
10.0
100
1000

FIGURE 9

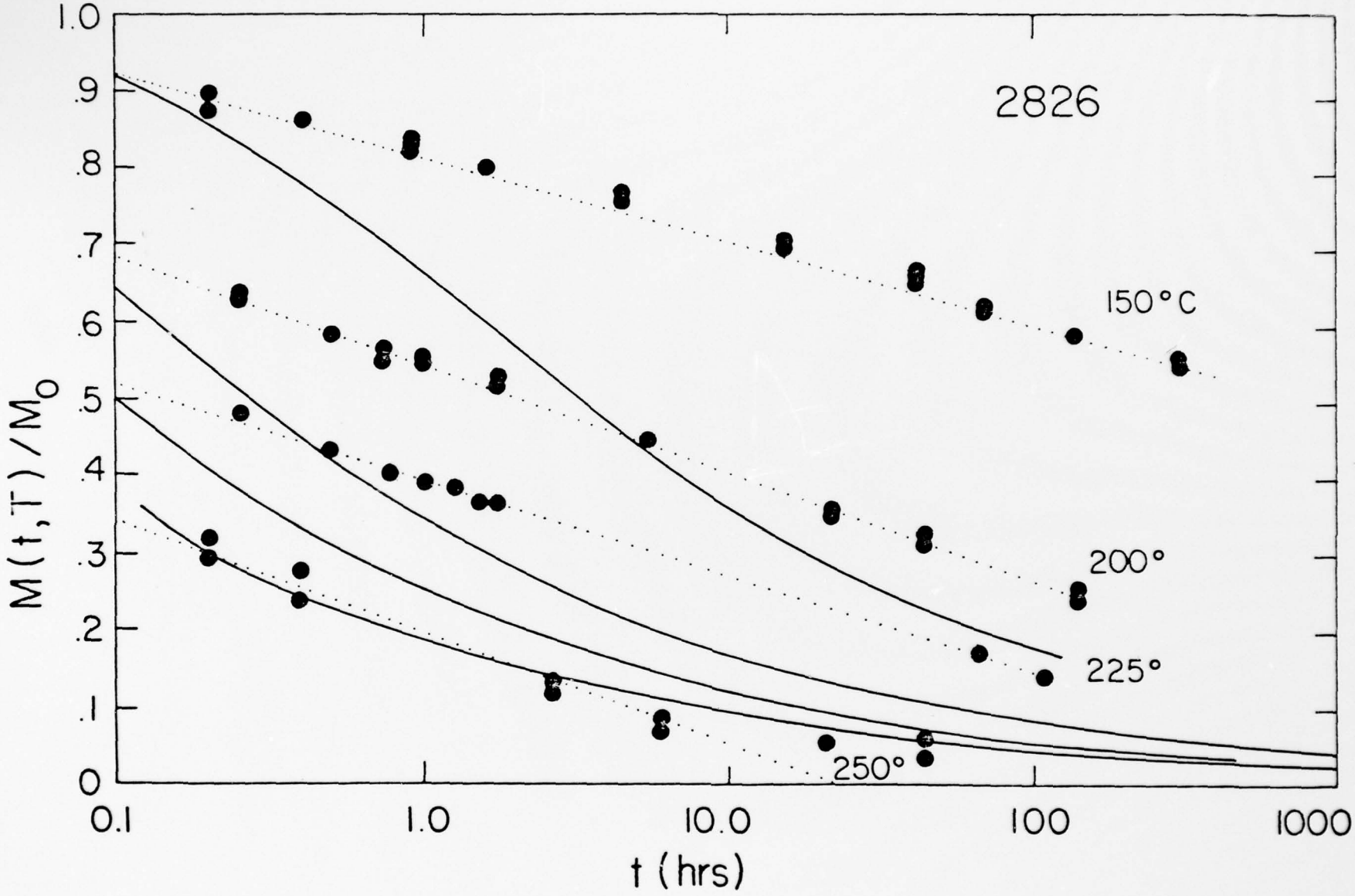
2826
150°C
200°
225°
250°
M(t,T)/M0
t (hrs)
1.0
.9
.8
.7
.6
.5
.4
.3
.2
.1
0
0.1
1.0
10.0
100
1000

FIGURE 10

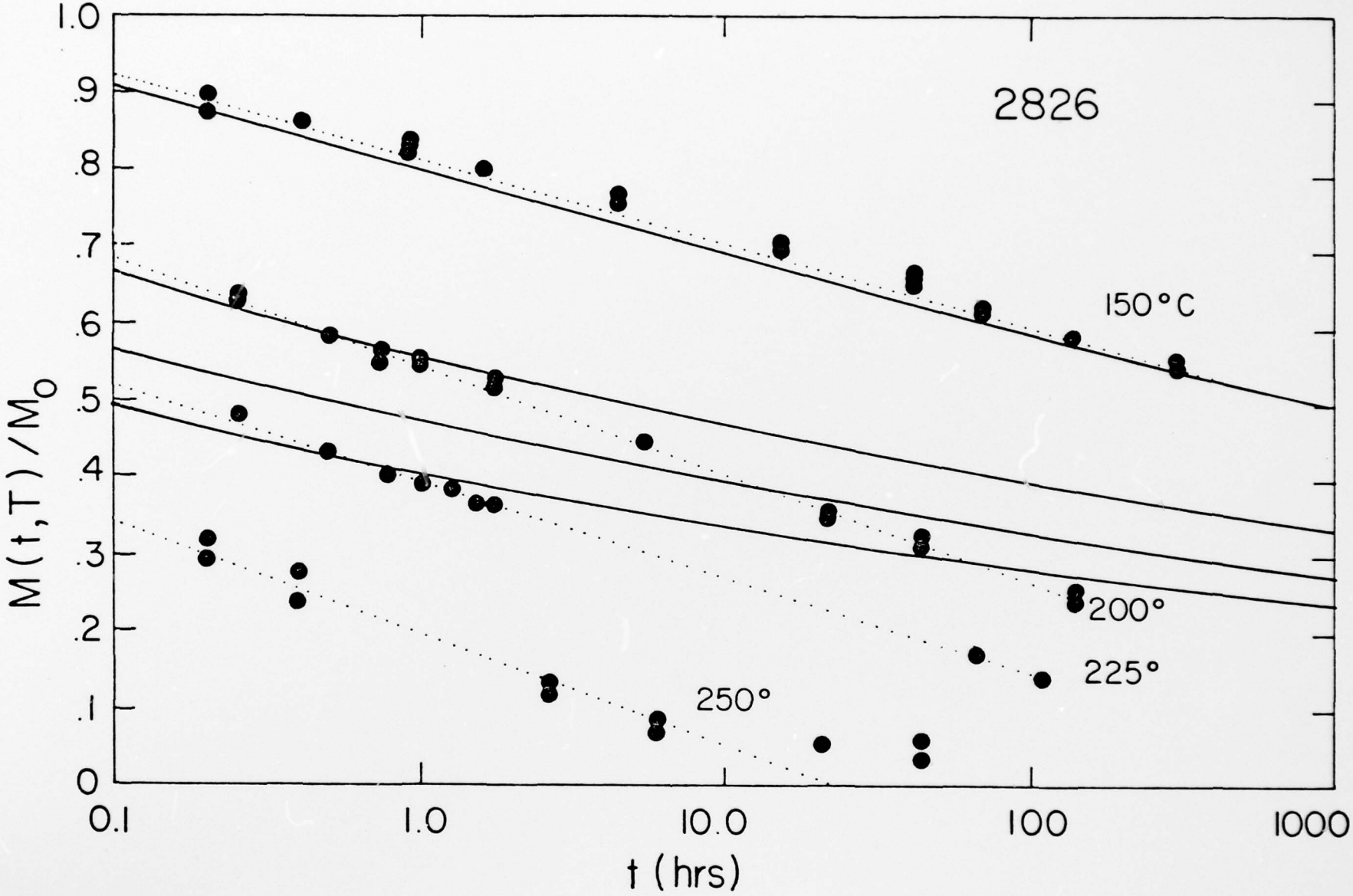
2826
150°C
200°
225°
250°
M(t,T)/M0
t (hrs)
1.0
.9
.8
.7
.6
.5
.4
.3
.2
.1
0
0.1
1.0
10.0
100
1000

FIGURE 11

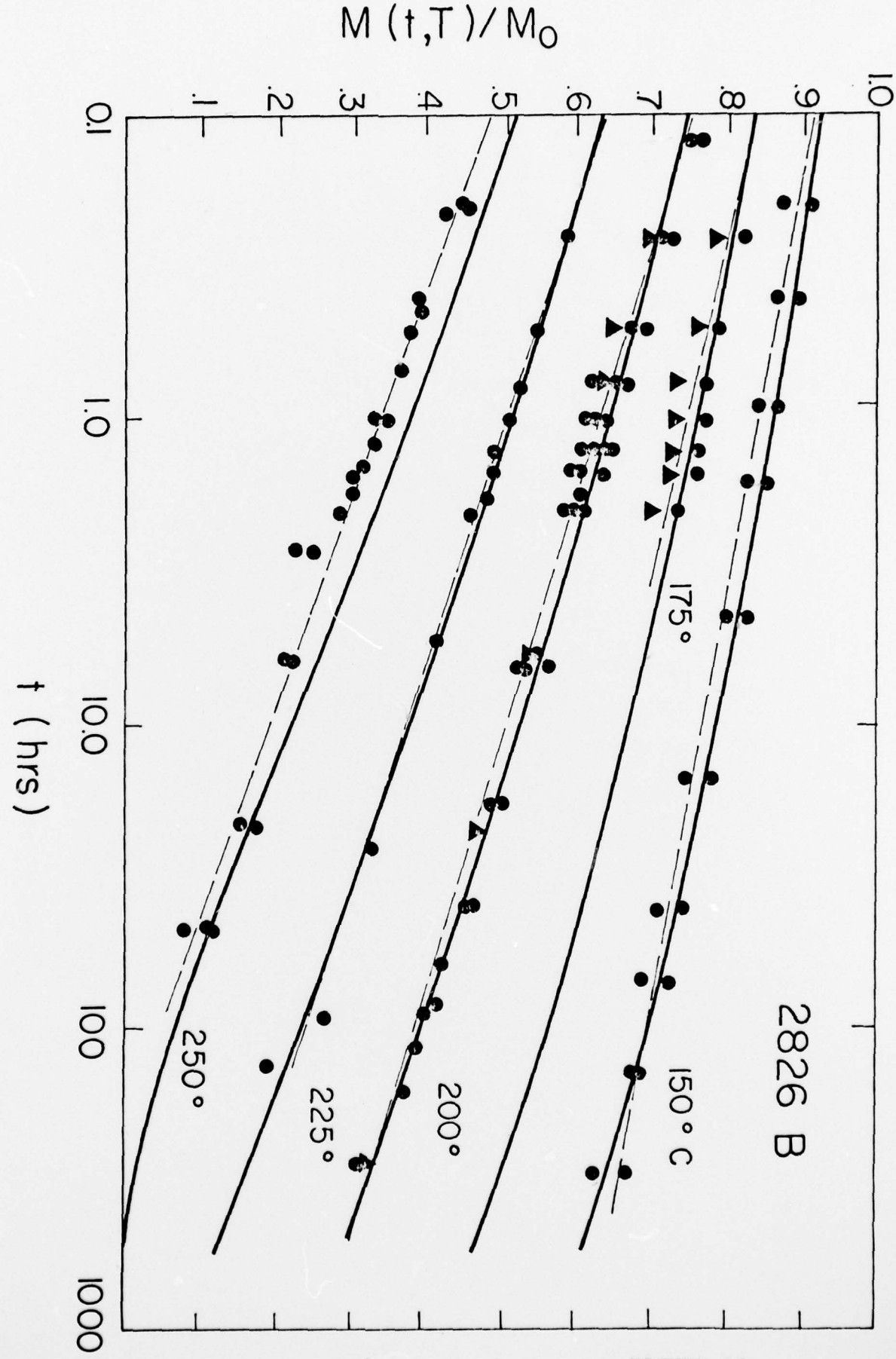
M (t,T) / M0
.1
.2
.3
.4
.5
.6
.7
.8
.9
1.0
0.1
1.0
10.0
100
1000
t (hrs)
250°
225°
200°
175°
150° C
2826 B

FIGURE 12

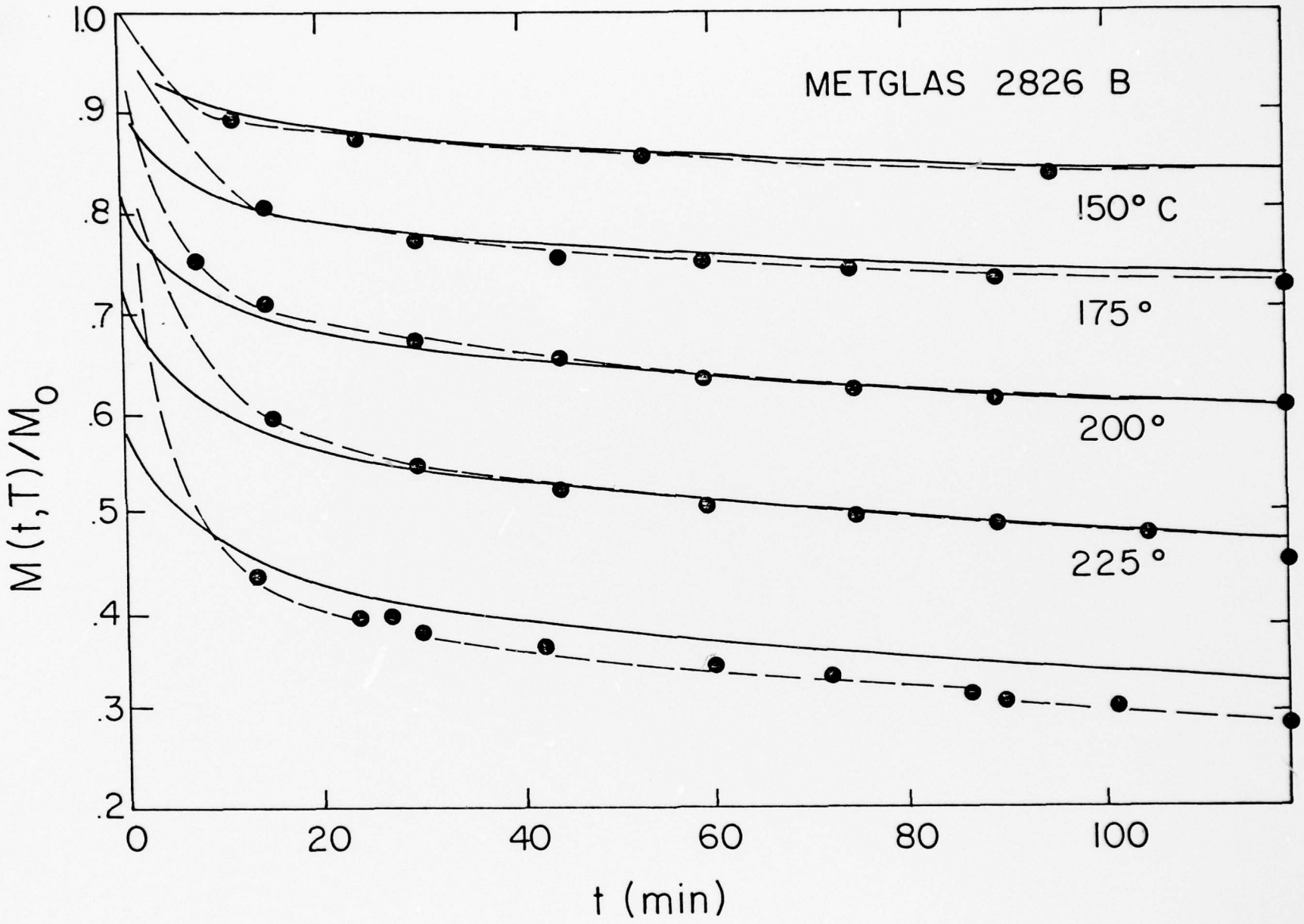
METGLAS 2826 B
150° C
175°
200°
225°
M(t,T)/M0
t (min)
1.0
.9
.8
.7
.6
.5
.4
.3
.2
0
20
40
60
80
100

FIGURE 13

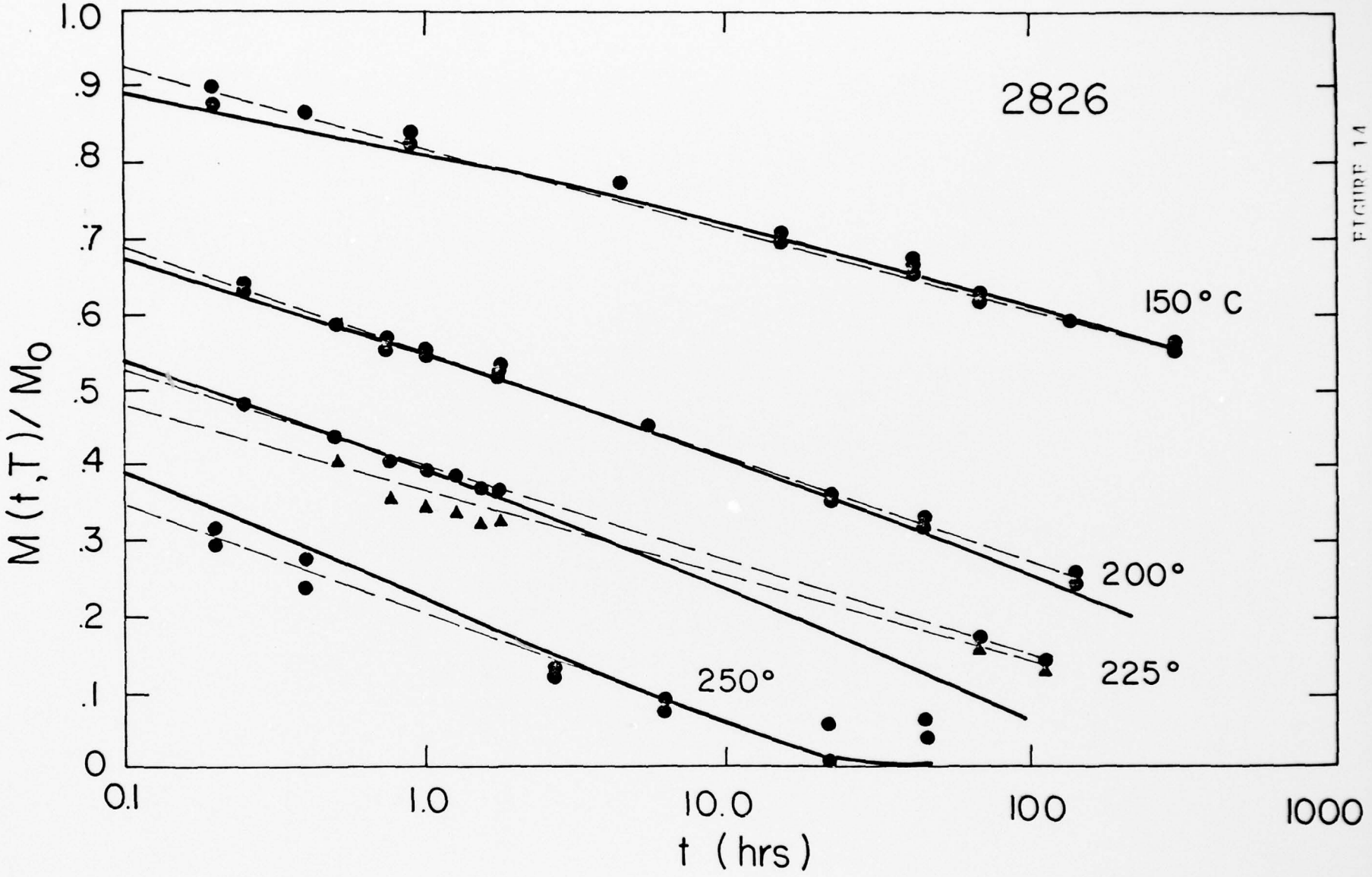
2826
150° C
200°
225°
250°
M (t,T) / M0
t (hrs)
1.0
.9
.8
.7
.6
.5
.4
.3
.2
.1
0
0.1
1.0
10.0
100
1000

FIGURE 14

BASIC DISTRIBUTION LIST

Technical and Summary Reports April 1978

Organization	Copies
Defense Documentation Center Cameron Station Alexandria, VA 22314	12
Office of Naval Research Department of the Navy 800 N. Quincy Street Arlington, VA 22217	
ATTN: Code 471	1
Code 102	1
Code 470	1
Commanding Officer Office of Naval Research Branch Office Building 114, Section D 666 Summer Street Boston, MA 02210	1
Commanding Officer Office of Naval Research Branch Office 536 South Clark Street Chicago, IL 60605	1
Office of Naval Research One Hallidie Plaza Suite 601 San Francisco, CA 94102	1
Naval Research Laboratory Washington, DC 20375	
ATTN: Codes 6000	1
6100	1
6300	1
6400	1
2627	1
Naval Air Development Center Code 302 Warminster, PA 18964 ATTN: Mr. F. S. Williams	1

Organization	Copies
Naval Air Propulsion Test Center Trenton, NJ 08628 ATTN: Library	1
Naval Construction Batallion Civil Engineering Laboratory Port Hueneme, CA 93043 ATTN: Materials Division	1
Naval Electronics Laboratory San Diego, CA 92152 ATTN: Electron Materials Sciences Division	1
Naval Missile Center Materials Consultant Code 3312-1 Point Mugu, CA 92041	1
Commanding Officer Naval Surface Weapons Center White Oak Laboratory Silver Spring, MD 20910 ATTN: Library	1
David W. Taylor Naval Ship Research and Development Center Materials Department Annapolis, MD 21402	1
Naval Undersea Center San Diego, CA 92132 ATTN: Library	1
Naval Underwater System Center Newport, RI 02840 ATTN: Library	1
Naval Weapons Center China Lake, CA 93555 ATTN: Library	1
Naval Postgraduate School Monterey, CA 93940 ATTN: Mechanical Engineering Department	1

BASIC DISTRIBUTION LIST (cont'd)

Organization	Copies
Naval Air Systems Command Washington, DC 20360 ATTN: Codes 52031 52032	1
Naval Sea System Command Washington, DC 20362 ATTN: Code 035	1
Naval Facilities Engineering Command Alexandria, VA 22331 ATTN: Code 03	1
Scientific Advisor Commandant of the Marine Corps Washington, DC 20380 ATTN: Code AX	1
Naval Ship Engineering Center Department of the Navy Washington, DC 20360 ATTN: Code 6101	1
Army Research Office P.O. Box 12211 Triangle Park, NC 27709 ATTN: Metallurgy & Ceramics Program	1
Army Materials and Mechanics Research Center Watertown, MA 02172 ATTN: Research Programs Office	1
Air Force Office of Scientific Research Bldg. 410 Bolling Air Force Base Washington, DC 20332 ATTN: Chemical Science Directorate Electronics & Solid State Sciences Directorate	1 1
Air Force Materials Laboratory Wright-Patterson AFB Dayton, OH 45433	1
Library Building 50, Rm 134 Lawrence Radiation Laboratory Berkeley, CA	1

Organization	Copies
NASA Headquarters Washington, DC 20546 ATTN: Code RRM	1
NASA Lewis Research Center 21000 Brookpark Road Cleveland, OH 44135 ATTN: Library	1
National Bureau of Standards Washington, DC 20234 ATTN: Metallurgy Division Inorganic Materials Div.	1 1
Director Applied Physics Laboratory University of Washington 1013 Northeast Forthieth Street Seattle, WA 98105	1
Defense Metals and Ceramics Information Center Battelle Memorial Institute 505 King Avenue Columbus, OH 43201	1
Metals and Ceramics Division Oak Ridge National Laboratory P.O. Box X Oak Ridge, TN 37380	1
Los Alamos Scientific Laboratory P.O. Box 1663 Los Alamos, NM 87544 ATTN: Report Librarian	1
Argonne National Laboratory Metallurgy Division P.O. Box 229 Lemont, IL 60439	1
Brookhaven National Laboratory Technical Information Division Upton, Long Island New York 11973 ATTN: Research Library	1
Office of Naval Research Branch Office 1030 East Green Street Pasadena, CA 91106	1

SUPPLEMENTARY DISTRIBUTION LIST

Technical and Summary Reports November 1978

Professor G. S. Ansell
Rensselaer Polytechnic Institute
Department of Metallurgical
Engineering
Troy, NY 12181

Professor Dieter G. Ast
Cornell University
Department of Materials Science
and Engineering
Ithaca, NY 14853

Dr. E. M. Breinan
United Technologies Corporation
United Technologies Research Center
East Hartford, CT 06108

Professor H. D. Brody
University of Pittsburgh
School of Engineering
Pittsburgh, PA 14213

Dr. R. W. Cahn
University of Sussex
School of Engineering and
Applied Science
Brighton BN1 9QT
ENGLAND

Dr. E. A. Clark
Solid State Division
Naval Surface Weapons Center
White Oak Laboratory
Silver Spring, MD 20910

Dr. S. M. Copley
University of Southern California
Los Angeles, CA 90007

Professor M. Cohen
Massachusetts Institute of Technology
Department of Metallurgy
Cambridge, MA 02139

Dr. R. B. Diegle
Battelle
505 King Avenue
Columbus, OH 43201

Professor B. C. Giessen
Northeastern University
Department of Chemistry
Boston, MA 02115

Professor N. J. Grant
Massachusetts Institute of Technology
Department of Materials Science
and Engineering
Cambridge, MA 02100

Dr. F. E. Luborsky
General Electric Company
P. O. Box 8
Corporate R&D
Schenectady, NY 12301

Dr. J. Perel
Phrasor Technology
1536 Highland Avenue
Duarte, CA 91010

Professor O. D. Sherby
Stanford University
Materials Science Division
Stanford, CA 94300

Professor D. Turnbull
Harvard University
Division of Engineering and
Applied Physics
Cambridge, MA 02138

Professor R. Mehrabian
University of Illinois
Department of Mechanical and
Industrial Engineering
Urbana, IL 61801

Professor P. R. Strutt
University of Connecticut
School of Engineering
Department of Metallurgy
Storrs, CT 06268